Energy transfer by a secondary acoustic source through Friction-Induced Vibrations: A power flow analysis

Soizic Terrien, Lucas Frache, Eric Chatelet, Francesco Massi

Version of Record: https://www.sciencedirect.com/science/article/pii/S0022460X19305243
Manuscript_d62250cc8d46f13a88f1e8344a9fafbb

Energy transfer by a Secondary Acoustic Source through Friction-Induced Vibrations : a power flow analysis

Soizic Terrien

Univ Lyon, INSA-Lyon, CNRS UMR5259, LaMCoS, F-69621, France

Lucas Frache

Univ Lyon, INSA-Lyon, CNRS UMR5259, LaMCoS, F-69621, France

Eric Chatelet

Univ Lyon, INSA-Lyon, CNRS UMR5259, LaMCoS, F-69621, France

Francesco Massi

DIMA, Department of Mechanical and Aerospace Engineering, University of Rome La Sapienza, Italy

Abstract

Friction Induced Vibrations occur in many different contexts, from automotive industry to musical instruments, and are often investigated for their detrimental effects such as surface damage and dynamical instabilities. In this article, a mechanical device exploits Friction Induced Vibrations to transfer energy in a structure from a *primary* ambient low-frequency vibrational field towards a *secondary* acoustic field with a higher and wider frequency content. This device constitutes a Secondary Acoustic Source for the structure. An approach is proposed to quantify the energy flow between the primary and secondary acoustic fields from the sole measurement of acceleration signals at a finite number of points on the experimental structure. These results pave the way towards the optimisation of the energy transfer by the Secondary Acoustic Source and, as such, towards its use for Structural Health Monitoring applications.

1. Introduction

Friction-Induced Vibrations (FIV) is a general, widespread phenomenon, observed in contexts as different as squeal of vehicle brakes [10, 7, 27, 23, 13], squeak of hip prosthetics [24, 29, 21, 9], tactile perception [8, 5, 19] and sound production by bowed-string instruments [16, 30]. Physically, FIV result from the dynamic excitation of a structure by a contact interface [17, 1, 4], and are affected by both system and contact characteristics. Although most studies focused on the detrimental effects of FIV including wear, surface damage, fatigue, noise and dynamical instabilities [12, 22, 7], recent works focused on the control and exploitation of FIV, for example to harvest or transfer vibrational energy [15, 4].

In this context, this article focuses on the use of FIV to transfer acoustic energy from a low frequency acoustic (vibrational) field in a structure towards a secondary acoustic field with a higher and wider spectral content. To this aim, a Secondary Acoustic Source (SAS) has been developed in the form of a mechanical device composed of two resonators coupled through a frictional interface (Figure 1). The primary resonator aims at harvesting energy from the ambient noise, and, as such, is designed so that its natural frequency is within the frequency range of the ambient acoustic field. The vibrational response of the primary resonator results in a relative motion at the interface with the secondary oscillator. This frictional interface causes a broadband excitation, and, hence, produces a secondary acoustic field with a higher and wider spectral content. Altogether, the SAS is expected to behave as a localised, high-frequency secondary source for the structure.

The developed SAS is expected to be of particular interest for applications in Structural Health Monitoring (SHM), which aims at detecting and localising damages and defects in structures and is, as such, of crucial importance in aeronautics and civil engineering [6, 25]. Classical active approaches in SHM rely on the characterisation of changes in the response of a structure to an external excitation [26]. The associated power consumption constitutes a major limitation for their application to continuous monitoring of structural health. Alternatively, passive techniques aim at using the ambient noise in the structure to detect defects and damages [18, 28], without the need for active acoustic sources. Important technical limitations lie in the availability of suitable noise sources : indeed, passive SHM techniques require uncorrelated, wideband, high-frequency noise sources with fixed locations. In this context, the role of the Secondary Acoustic Source is to harvest energy from the non-stationary, low frequency ambient acoustic field (e.g. vibrations from engines on an aircraft wing), and to transfer it towards a higher wideband frequency range, by exploiting the broadband excitation generated at the frictional interface [4].

A preliminary study provided the proof of concept for this approach [3]. The optimisation of the energy transfer between the ambient and the secondary acoustic fields is now an essential step towards applications in SHM. This implies first to quantify the energy flow between the SAS and the structure, and, as a second step, to investigate the influence, on this energy flow, of the SAS parameters. This includes the dynamic parameters of the two resonators, such as their mass and stiffness, as well as the parameters associated with the frictional interface, such as surface roughness and normal contact force.

In this article, we propose a method to quantify the energy transfer between the ambient low-frequency acoustic field and the secondary acoustic field. This allows to perform a preliminary study on the influence of the normal contact force at the frictional interface on the energy transfer. The article is organised as follows. The experimental setup is described in section 2. The power flow estimation method is detailed and validated in section 3. Section 4 presents preliminary results on the influence of the force at the contact interface of the SAS on the power flow and energy transfer. Finally, the results are discussed in section 5.

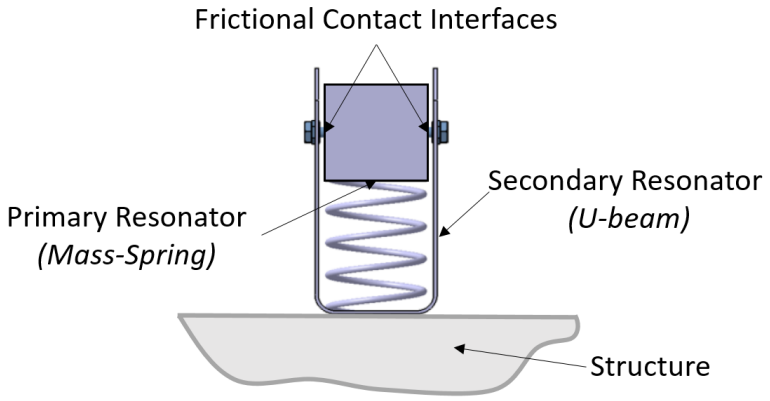

Figure 1: Schematic representation of the Secondary Acoustic Source (SAS). A main resonator, constituted by a spring of stiffness 2710 N/m and a 7.5mm aluminium cube, is in frictional contact through two screw heads with a $27.5 \times 7.5 \times 0.5$mm U-shaped steel beam (the secondary resonator). The contact condition can be changed by adjusting the two screws tightness.

2. Experimental setup

The experimental setup is represented in Figure 2. A free-free 500mm long, 300 mm wide, 3mm thick aluminium plate (the structure) is excited by a shaker at Point 1, with a low-frequency, narrow-band noise, between 50Hz and 130Hz. This represents a structure subject to an ambient acoustic field. The Secondary Acoustic Source is connected to the plate at Point 2. Two force sensors, a PCB 208C01 and a B&K type 8200 are connected to the structure at points 1 and 2, respectively, together with two accelerometers PCB 353B18 and PCB352A24, respectively. A third accelerometer B&K 4397 is located at point 3, far from both the shaker and the SAS, in order to estimate the ability of the SAS to affect the frequency content of the acoustic field in the whole structure. The data acquisition is realised through a LMS acquisition system with a sample frequency of 25.6 kHz.

Figure 1 represents the SAS in more details. The main resonator is composed of a spring of stiffness 2710 N/m and an aluminium cube of 7.5mm side length. It is in frictional contact through two screw heads with the secondary resonator, a U-shaped steel beam. The normal force at the sliding interfaces between the two resonators is controled by adjusting the screws tightness. The resonance frequency of the main resonator is around 80 Hz, in the frequency range of the ambient noise (provided by the shaker) and close to a natural frequency of the plate. The frequency of the first bending mode of the U-shaped beam is around 303 Hz.

The idea behind this SAS is the following: the ambient noise induces oscillations of the main resonator, which results in a frictional contact at the rough interface with the secondary resonator, thus providing a wideband excitation to this secondary resonator [2]. Under the assumption of a weak contact, one can expect that the secondary resonator will respond to this excitation with its own natural frequencies [20], and reinject energy in the plate. The SAS would thus constitute a *secondary* wideband, high-frequency noise source for the structure.

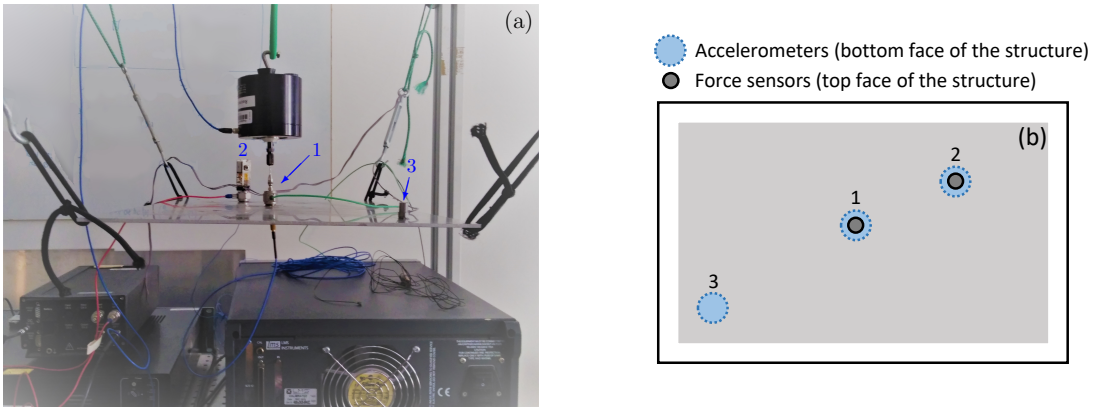

Figure 2: (a) Photography and (b) schematic top view of the experimental setup : the structure (a 500mm long, 300mm wide, 3mm thick aluminium plate) is excited at point 1 by a shaker with a filtered white noise, with a frequency content between 50Hz and 130Hz. The Secondary Acoustic Source (SAS) is located at point 2. The force and acceleration are measured at points 1 and 2, and a third accelerometer is located at point 3, far from both sources.

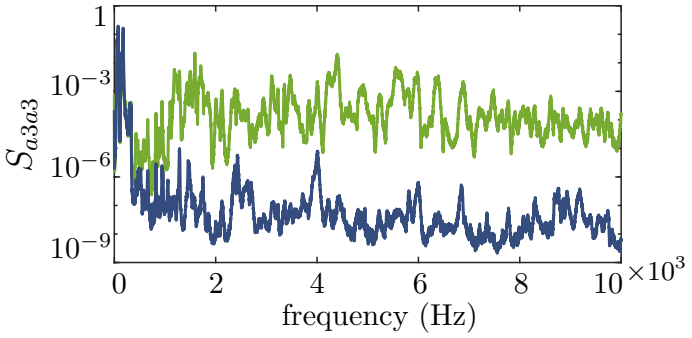

Figure 3: Power spectral density S_{a3a3} of the acceleration measured at point 3 (logarithmic scale), without contact (blue curve) and with frictional contact (green curve) between the two resonators of the Secondary Acoustic Source.

2.1. Energy transfer towards higher frequencies

Figure 3 represents the Power Spectral Density (PSD) S_{a3a3} of the acceleration measured at point 3 (*i.e.* far from both the shaker and the SAS), for two different configurations of the SAS, namely when its two resonators are not in contact (*i.e.* the SAS is not activated), and when they are in frictional contact (*i.e.* the SAS is activated). The statistical properties of the excitation signal provided by the shaker are identical in both cases. In figure 3, the frequency content of the ambient noise in the structure differs significantly between the two cases. In particular, the energy content is significantly higher in the frequency range [350,10000]Hz when the two resonators of the SAS are in frictional contact (green curve), compared to the case without contact (blue curve).

3. Quantification of the energy flow between the structure and the SAS

These preliminary results demonstrate the ability of the SAS to transfer energy from the low-frequency, narrow-band ambient acoustic field towards a *secondary* acoustic field with a higher and wider spectral content. Importantly, a single SAS is able to affect the frequency content of the ambient acoustic field in the whole structure. The optimisation of this energy transfer is an essential step towards applications in SHM. This implies to investigate the effect of both the contact parameters (normal force at contact and interface roughness) and the resonators geometry (stiffness and mass) on the efficiency of the energy transfer. A first step of the optimisation process is the quantification of the power flow between the vibrating plate (the structure) and the SAS.

Assuming that the SAS does not significantly affect the plate dynamics [11, 3], one can consider that the structure is subject to two external forces $f_1(t)$ and $f_2(t)$ applied by the shaker at point 1 and the SAS at point 2, respectively. Considering moreover, in first approximation, that both $f_1(t)$ and $f_2(t)$ are point forces, the power flow $< P_2 >$ at point 2 is written as follows [20, 14]:

$$< P_2 >= \frac{1}{2\pi} \int_{-\infty}^{\infty} Re(S_{f_2 v_2}(\omega)) d\omega. \tag{1}$$

Here, $S_{f_2 v_2}(\omega)$ is the cross power spectral density (CPSD) of the force $f_2(t)$ and the velocity $v_2(t)$ measured at point 2. It is straightforward to retrieve $S_{f_2 v_2}(\omega)$ from the measured acceleration and force signals ($a_2(t)$ and $f_2(t)$, respectively):

$$S_{f_2 v_2}(\omega) = \frac{1}{i\omega} S_{f_2 a_2}(\omega). \tag{2}$$

Throughout this article, two distinct frequency bands are considered for the integration of equation (1). In the one hand, the *excitation frequency band* [50,130]Hz, which corresponds to the frequency range of the ambient low-frequency narrow-band noise provided by the shaker. On the other hand, the *higher frequency band* [1000,10000]Hz is of interest in the context of SHM, and corresponds to the frequency range in which acoustic energy is transferred by the sliding contact (see Figure 3). Hereafter, the ability of the SAS to reinject energy in the plate is evaluated on the higher frequency band. The comparison of the power flow in these two frequency bands gives an estimation of the *efficiency* of the SAS, that is to say its ability to harvest energy from the ambient acoustic field and to convert and reinject this energy in the higher frequency band.

Figure 4 represents the value of $< P_2 >$ on these two frequency bands, for the two cases considered in Figure 3, corresponding to a deactivated SAS (*i.e* there is no contact between its two resonators) and an activated SAS (*i.e.* the two resonators are in sliding contact), respectively. Here, a negative sign means that energy is flowing from the plate towards the SAS while a positive sign means that the SAS is injecting energy into the structure. In the excitation frequency band, no significant difference is observed between the two cases : both with and without contact, the negative sign of $<P_2>$ shows that the SAS harvests energy from the structure. In the higher frequency band, as expected, no energy transfer is observed between the

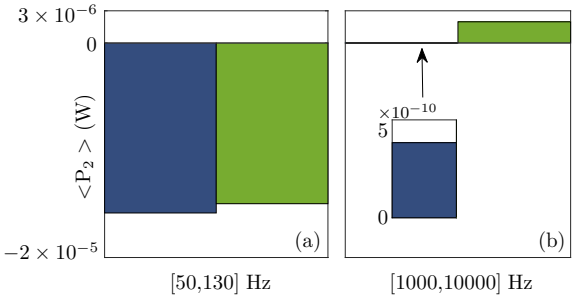

Figure 4: Power $<P_2>$ (W) between the plate and the SAS, for the cases without (blue) and with (green) contact between the two resonators of the SAS. Shown are (a) the power flow in the excitation band [50,130] Hz and (b) in the higher frequency band [1000,10000] Hz.

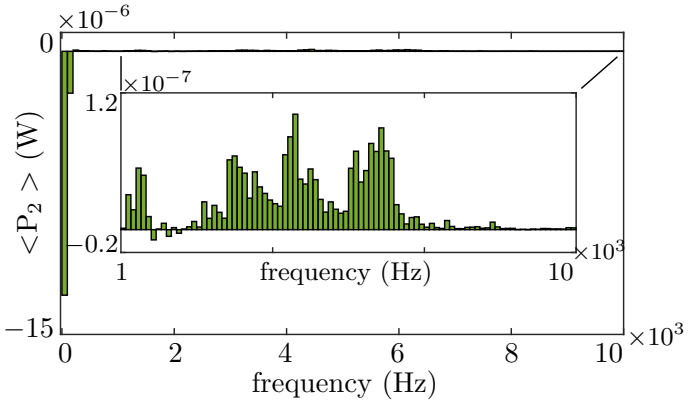

Figure 5: Power $<P_2>$ (W) between the plate and the SAS, integrated on 100Hz-wide frequency bands. The two resonators of the SAS are in frictonal contact. The inset shows a zoom on the higher frequency band [1000,10000] Hz.

structure and the SAS when the SAS is not activated. When it is activated, on the other hand, Figure 4 clearly shows that the SAS injects energy into the structure. The power flow is represented in more details in Figure 5, where the power $<P_2>$ is now integrated over 100 Hz - wide frequency bands. This demonstrates clearly that the plate injects energy in the SAS almost exclusively below 200 Hz. Above 1000 Hz on the other hand, the SAS constitutes a secondary acoustic source which injects energy in the structure.

3.1. Estimation of the power flow from acceleration signals only

Quantifying the power flow at point 2 from equation (1) requires the simultaneous measurement of the force and acceleration signals $f_2(t)$ and $a_2(t)$. Force sensors are not compact, and the need for measuring both the force and acceleration is an important limitation in the context of applications, where several dozens of SAS will be typically used simultaneously [3]. Moreover, one can expect that introducing the force sensor between the SAS and the plate might affect the efficiency of the energy transfer. We show here that the power flow $< P_2 >$ can be estimated accurately using the acceleration signals only.

Under the assumption of sufficiently small vibration amplitude, the vibrating structure can be considered as a multiple input - multiple output linear, time-invariant system, where the inputs are the (external) forces $f_1(t)$ and $f_2(t)$ applied by the shaker and the SAS, respectively, and the outputs are the acceleration signals $a_1(t)$ and $a_2(t)$. The response of such a system to a random excitation is defined as follows [14] :

$$\mathbf{S_{aa}}(\omega) = \overline{\mathbf{H}}(\omega)\mathbf{S_{fa}}(\omega). \tag{3}$$

Here, $\mathbf{S_{aa}}(\omega)$ is the matrix of power spectral densities of the accelerations (output), $\mathbf{H}(\omega)$ is the matrix of the frequency response functions of the structure, and $\mathbf{S_{fa}}(\omega)$ is the matrix of the force - acceleration (input - output) cross power spectral densities. Because we consider here a two inputs - two outputs system, these are 2×2 matrices:

$$\mathbf{S_{aa}}(\omega) = \begin{bmatrix} S_{a_1a_1}(\omega) & S_{a_1a_2}(\omega) \\ S_{a_2a_1}(\omega) & S_{a_2a_2}(\omega) \end{bmatrix}, \tag{4}$$

$$\mathbf{H}(\omega) = \begin{bmatrix} H_{11}(\omega) & H_{12}(\omega) \\ H_{21}(\omega) & H_{22}(\omega) \end{bmatrix}, \tag{5}$$

$$\mathbf{S_{fa}}(\omega) = \begin{bmatrix} S_{f_1a_1}(\omega) & S_{f_1a_2}(\omega) \\ S_{f_2a_1}(\omega) & S_{f_2a_2}(\omega). \end{bmatrix}, \tag{6}$$

The matrix of the force - velocity cross power spectral densities $\mathbf{S_{fv}}(\omega)$ can be calculated by inverting the matrix $\mathbf{H}(\omega)$ in equation (3):

$$\begin{aligned} \mathbf{S_{fv}}(\omega) &= \frac{1}{i\omega}\mathbf{S_{fa}}(\omega) \\ &= \frac{1}{i\omega}\overline{\mathbf{H}}^{-1}(\omega)\mathbf{S_{aa}}(\omega) \\ &= \overline{\mathbf{M}}^{-1}(\omega)\mathbf{S_{aa}}(\omega), \end{aligned} \tag{7}$$

where $\mathbf{M}(\omega)$ is the mobility matrix of the vibrating structure.

Importantly, the use of the transfer matrix, which is designed for linear systems, is based on the assumption that the SAS is considered here as an external excitation source which provides an excitation to the structure. As such, the proposed method does not model the nonlinear phenomena at the contact interface between the resonators of the SAS. The dynamic contribution of the whole SAS, as well as the one of the shaker, are neglected and the transfer matrix is considered as the one of the structure alone, between the points where the SAS and shaker are connected to the structure. This assumption is supported by preliminary experimental results [11] and will be corroborated hereafter by comparing the power flow calculated from the measured force and acceleration signals on the one hand (equations (1) and (2)), and retrieved from the transfer matrix and the acceleration signals only on the other hand (equations (1) and (7)).

3.1.1. Estimation of the frequency response function

The frequency response functions $H_{ij}(\omega)$ are estimated from the simultaneous measurement of forces and accelerations at points 1 (shaker) and 2 (SAS). The structure is excited by the shaker with a wideband noise on the whole frequency

band [30,10000] Hz. The first and secondary resonators of the SAS are in frictional contact so that the SAS constitutes a wideband external source for the structure, as demonstrated in the previous section (see Figure 5).

The frequency response matrix of the two inputs - two outputs linear system is calculated using the estimator $H1$ [14]:

$$\overline{\mathbf{H}}(\omega) = \mathbf{S_{af}}(\omega)\mathbf{S_{ff}}^{-1}(\omega) \tag{8}$$

where $\overline{\mathbf{H}}(\omega)$ is the complex conjugate matrix of $\mathbf{H}(\omega)$, $\mathbf{S_{ff}}(\omega)$ is the matrix of power spectral densities of the force signals, $\mathbf{S_{af}}(\omega)$ is the matrix of the acceleration - force cross power spectral densities

3.1.2. Validation of the method

Figure 6 represents the cross power spectral density (CPSD) $S_{f_2v_2}(\omega)$ calculated directly from the measured acceleration and force temporal signals $a_2(t)$ and $f_2(t)$ on the one hand, and retrieved from the accelerations signals $a_1(t)$ and $a_2(t)$ and the frequency response functions using equation (7) on the other hand. The contact conditions between the two resonators of the SAS are unchanged compared to the measurement conditions of the frequency response functions. As before, the structure is excited by the shaker with a low frequency, narrow-band noise in the frequency band [50,130]Hz. Overall, the measured and retrieved CPSD $S_{f2v2}(\omega)$ in Figure 6 show good qualitative and quantitative agreement.

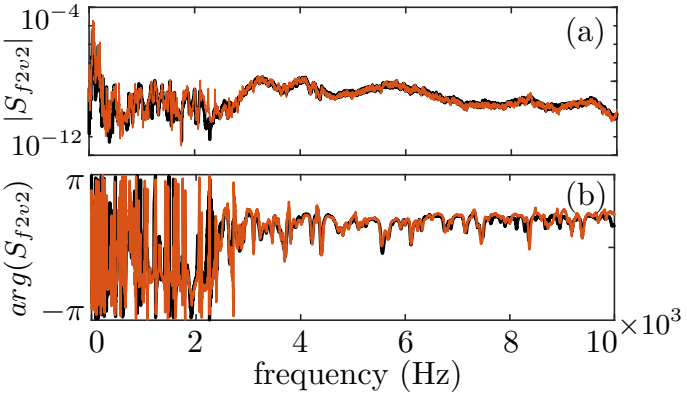

Figure 6: Modulus (a) and phase (b) of the measured (black) and retrieved (red) cross power spectral density $S_{f_2v_2}$, with respect to the frequency. The plate is excited by the shaker in the frequency band [50,130] Hz and the contact conditions between the two resonators of the SAS are identical to the one considered for the measurement of the frequency response functions.

In order to fully validate the transfer matrix method, we now use the retrieved function $S_{f_2v_2}(\omega)$ to estimate the power $< P_2 >$ supplied by the SAS to the structure in the high frequency band. In figure 7, the results are compared with the value of $< P_2 >$ calculated from the measured force and acceleration signals. This shows that in the high frequency band, where acoustic energy is transferred by the frictional contact between the two resonators of the SAS, the retrieved and measured values of $< P_2 >$ differ by less than 2%. The right panel in Figure 7 represents the measured and retrieved power $< P_2 >$ integrated over 100Hz-wide frequency

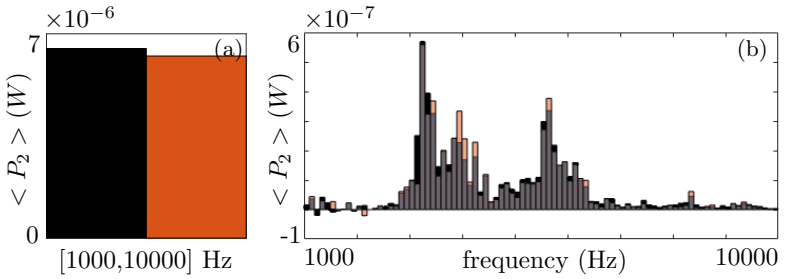

Figure 7: Measured (black) and retrieved (red) power flow $<P_2>$ (W) integrated over the high frequency band (a) and over 100Hz-wide frequency bands (b). The experimental conditions are identical to the one considered in Figure 6.

bands, thus allowing for a more comprehensive comparison. Overall, the measured and retrieved results show excellent qualitative and quantitative agreement, which strongly suggests that the power flow between the SAS and the structure can be estimated accurately from the sole measurement of the accelerations signals at the source points.

4. Influence of the contact force

In this section, we investigate the influence of the normal force at the contact interface between the two resonators of the SAS both on the accuracy of the proposed methof for the estimation of the power flow between the structure and SAS, and on the efficiency of the energy transfer by the SAS. In addition to the contact conditions considered in Figure 6 and 7, two qualitatively different values of the normal force at the contact interface are considered. The power $<P_2>$ exchanged between the SAS and the structure is estimated from the measured accelerations only using the method presented in section 3.1, and the results are compared with the values calculated from the measured force and acceleration signals. Importantly, the frequency response functions (FRF) considered for retrieving the CPSD $S_{f_2v_2}$ (and then the power flow $<P_2>$) are the same as considered in the previous section : these are thus measured for different contact conditions than the one considered hereafter. This allows to assess the reliability of the proposed power flow estimation method for a set of different contact conditions, while using a single set of FRF measurement for different contact conditions.

The different values of the contact force at the frictional interface are obtained by changing the revolution number of the screws (see figure 1). In addition to the case presented in the previous section, two further cases are considered, which correspond to a weaker and stronger normal force at contact.

4.0.1. Weaker contact force

Figure 8 shows the measured and retrieved value of $< P_2 >$, when the normal force at the contact interface between the two resonators of the SAS is weaker than the one considered for the measurement of the FRF. It is important to note that we

consider here very small values of the normal force at contact (estimated below 0.03 N). As before, the measured and retrieved data in Figure 8 show excellent agreement, and the retrieved value of $<P_2>$ in the high-frequency band [1000,10000]Hz differs by less than 1.3% from its measured value.

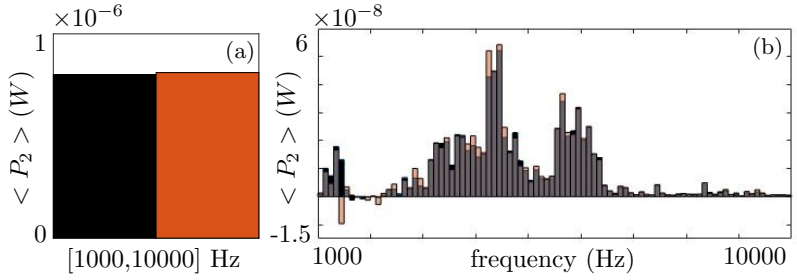

Figure 8: Power $<P_2>$ (W) exchanged between the structure and the SAS in the frequency band [1000,10000] Hz (a) and integrated over 100 Hz - wide frequency bands (b), for a weak normal force at the contact interface between the SAS resonators. Shown are the values calculated from the measured force and acceleration signals (black) and retrieved from the acceleration signals only (red).

4.0.2. Stronger contact force

Figure 9 represents similar results, when the normal force at the contact interface is larger than the one considered for the measurement of the FRF. As before, the agreement is excellent, and the relative difference between the measured and retrieved values of $<P_2>$ is below 3.5% in the high-frequency band.

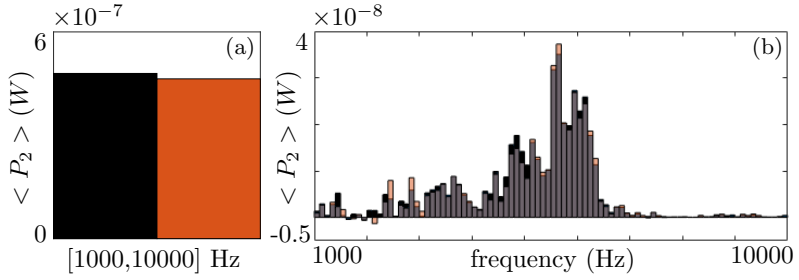

Figure 9: Power $< P2 >$ (W) exchanged between the structure and the SAS, in the frequency band [1000,10000] Hz (a) and integrated over 100 Hz - wide frequency bands (b), for a strong normal force at the contact interface between the SAS resonators. Shown are the values calculated from the measured force and acceleration signals (black) and retrieved from the acceleration signals only (red).

5. Discussion

The results presented here show how the designed Secondary Acoustic Source is able to transfer acoustic energy from the low-frequency narrow-band ambient noise

towards a secondary acoustic field with a higher and wider spectral content. As such, the SAS constitutes a passive source of acoustic energy, stationary in space and with a high-frequency acoustic signature. As shown in Figures 7, 8 and 9, the power flow between the designed SAS and the structure can be calculated accurately from the measurement of the sole acceleration signals at the two source points (here, the shaker and the SAS). Importantly, a single set of frequency response functions (FRF) is used for the estimation of the power flow, no matter what the contact conditions are between the SAS resonators. In fact, what is important is that the SAS is effectively a wideband noise source for the structure when the FRF are measured. These results are of particular interest for the optimisation of the secondary acoustic source in terms of energy transfer. In particular, this will allow a more in-depth investigation of the influence of the contact parameters on the energy transfer, without using force sensors apart from the initial FRF measurement.

In particular, our preliminary results suggests that the normal force at the contact interface has a significant influence on the energy towards high frequencies. The results presented in Figures 7, 8 and 9 highlight that, for a given excitation level of the structure by the shaker (*i.e.* a given level of ambient noise), the value of $<P_2>$ (and then the acoustic energy transfer) in the high frequency band is 8 to 13 times larger for the medium contact force than for the weak and strong contact force. This strongly suggests that a more in-depth parametric study would be particularly valuable in order to optimise the energy transfer.

Finally, for sake of clarity and simplicity, the proposed power flow estimation method has been considered so far for a single SAS. However, this technique will be of particular interest in the context of SHM, where several SAS will be used simultaneously [3].

6. Conclusions

This work demonstrates that a passive Secondary Acoustic Source is able to transfer acoustic energy from a low frequency ambient noise in a structure towards a higher and wider frequency band. An approach for estimating the energy flow between the SAS and the structure, and then the efficiency of the SAS, has been proposed and validated, which rely on the measurement of the acceleration signals only. A preliminary investigation of the influence of the normal force at the contact interface between the two SAS resonators highlighted the strong influence of this parameter on the efficiency of the energy transfer. Overall, these results pave the way towards a more comprehensive parametric study, and as such towards the optimisation of a Secondary Acoustic Source for applications in passive SHM. In particular, the need for a passive external acoustic source with a fixed spatial location and uncorrelated high frequency content will be satisfied by the SAS.

7. Acknowledgments

This work was supported by the project PANSCAN ANR-17-CE08-0013, funded by the french Agence Nationale de la Recherche (ANR).

References

[1] Abdelounis, H. B., Le Bot, A., Perret-Liaudet, J., and Zahouani, H. An experimental study on roughness noise of dry rough flat surfaces. *Wear 268*, 1-2 (2010), 335–345.

[2] Akay, A. Acoustics of friction. *The Journal of the Acoustical Society of America 111*, 4 (2002), 1525–1548.

[3] Chehami, L., Moulin, E., De Rosny, J., Prada, C., Chatelet, E., Lacerra, G., Gryllias, K., and Massi, F. Nonlinear secondary noise sources for passive defect detection using ultrasound sensors. *Journal of sound and Vibration 386* (2017), 283–294.

[4] Di Bartolomeo, M., Lacerra, G., Baillet, L., Chatelet, E., and Massi, F. Parametrical experimental and numerical analysis on friction-induced vibrations by a simple frictional system. *Tribology International 112* (2017), 47–57.

[5] Fagiani, R., Massi, F., Chatelet, F., Berthier, Y., and Akay, A. Tactile perception by friction induced vibrations. *Tribology International 44*, 10 (2011), 1100–1110.

[6] Farrar, C. R., and Worden, K. An introduction to structural health monitoring. *Philosophical Transactions of the Royal Society A: Mathematical, Physical and Engineering Sciences 365*, 1851 (2006), 303–315.

[7] Hoffmann, N., Fischer, M., Allgaier, R., and Gaul, L. A minimal model for studying properties of the mode-coupling type instability in friction induced oscillations. *Mechanics Research Communications 29*, 4 (2002), 197–205.

[8] Hollins, M., and Risner, S. R. Evidence for the duplex theory of tactile texture perception. *Perception & psychophysics 62*, 4 (2000), 695–705.

[9] Hothan, A., Huber, G., Weiss, C., Hoffmann, N., and Morlock, M. The influence of component design, bearing clearance and axial load on the squeaking characteristics of ceramic hip articulations. *Journal of biomechanics 44*, 5 (2011), 837–841.

[10] Ibrahim, R. Friction-induced vibration, chatter, squeal, and chaos - part i: mechanics of contact and friction. *Applied Mechanics Reviews 47*, 7 (1994), 209–226.

[11] Lacerra, G., Massi, F., Chatelet, E., and Moulin, E. Acoustic energy transfer by friction induced vibrations. *Procedia engineering 199* (2017), 1356–1361.

[12] Lazzari, A., Tonazzi, D., Conidi, G., Malmassari, C., Cerutti, A., and Massi, F. Experimental evaluation of brake pad material propensity to stick-slip and groan noise emission. *Lubricants 6*, 4 (2018,), 107.

[13] Lazzari, A., Tonazzi, D., and Massi, F. Squeal propensity characterization of brake lining materials through friction noise measurements. *Mechanical Systems and Signal Processing 128* (2019), 216–228.

[14] Le Bot, A. *Foundation of statistical energy analysis in vibroacoustics*. OUP Oxford, 2015.

[15] Le Bot, A., Bou-Chakra, E., and Michon, G. Dissipation of vibration in rough contact. *Tribology letters 41*, 1 (2011), 47–53.

[16] McIntyre, M., and Woodhouse, J. On the fundamentals of bowed-string dynamics. *Acta Acustica united with Acustica 43*, 2 (1979), 93–108.

[17] Meziane, A., Baillet, L., and Laulagnet, B. Experimental and numerical investigation of friction-induced vibration of a beam-on-beam in contact with friction. *Applied Acoustics 71* (2010), 843–853.

[18] Moulin, E., Abou Leyla, N., Assaad, J., and Grondel, S. Applicability of acoustic noise correlation for structural health monitoring in nondiffuse field conditions. *Applied Physics Letters 95*, 9 (2009), 094104.

[19] Ndengue, J. D., Cesini, I., Faucheu, J., Chatelet, E., Zahouani, H., Delafosse, D., and Massi, F. Tactile perception and friction-induced vibrations: Discrimination of similarly patterned wood-like surfaces. *IEEE transactions on haptics 10*, 3 (2017), 409–417.

[20] Norton, M. P., and Karczub, D. G. *Fundamentals of noise and vibration analysis for engineers*. Cambridge university press, 2003.

[21] Ouenzerfi, G., Massi, F., E, R., and Berthier, Y. Squeaking friction phenomena in ceramic hip endoprosthesis: Modeling and experimental validation. *Mechanical Systems and Signal Processing 58* (2015), 87–100.

[22] Ouyang, H., Nack, W., Yuan, Y., and Chen, F. Numerical analysis of automotive disc brake squeal: a review. *International Journal of Vehicle Noise and Vibration 1*, 3-4 (2005), 207–231.

[23] Sinou, J.-J. Transient non-linear dynamic analysis of automotive disc brake squeal–on the need to consider both stability and non-linear analysis. *Mechanics Research Communications 37*, 1 (2010), 96–105.

[24] Sinou, J.-J., Lenoir, D., Besset, S., and Gillot, F. Squeal analysis based on the laboratory experimental bench friction-induced vibration and noise at école centrale de lyon (five@ecl). *Mechanical Systems and Signal Processing 119* (2019), 561–588.

[25] Sohn, H., Farrar, C. R., Hemez, F. M., Shunk, D. D., Stinemates, D. W., Nadler, B. R., and Czarnecki, J. J. A review of structural health monitoring literature: 1996–2001. *Los Alamos National Laboratory, USA* (2003).

[26] Staszewski, W., Mahzan, S., and Traynor, R. Health monitoring of aerospace composite structures–active and passive approach. *composites Science and Technology 69*, 11-12 (2009), 1678–1685.

[27] Tonazzi, D., Massi, F., Baillet, L., Culla, A., Di Bartolomeo, M., and Berthier, Y. Experimental and numerical analysis of frictional contact scenarios: from macro stick–slip to continuous sliding. *Meccanica 50*, 3 (2015), 649–664.

[28] Tonazzi, D., Massi, F., Culla, A., Fregolent, A., and Berthier, Y. Role of damping on contact instability scenarios. In *5th World Tribology Congress, WTC* (2013).

[29] Weiss, C., Gdaniec, P., Hoffmann, N. P., Hothan, A., G, H., and M, M. M. Squeak in hip endoprosthesis systems: an experimental study and a numerical technique to analyze design variants. *Medical engineering & physics 32*, 6 (2010), 604–609.

[30] Woodhouse, J., and Galluzzo, P. The bowed string as we know it today. *ACTA Acustica united with Acustica 90*, 4 (2004), 579–589.